*Thermochimica Acta*, 66 (1983) 105–125
Elsevier Science Publishers B.V., Amsterdam – Printed in The Netherlands

# THERMAL DECOMPOSITION OF FERROMANGANOAN DOLOMITE

K. IWAFUCHI, C. WATANABE and R. OTSUKA

*Department of Mineral Industry, School of Science and Engineering, Waseda University, 3-4-1, Okubo, Shinjuku-ku, Tokyo (Japan)*

(Received 4 January 1983)

## ABSTRACT

This work investigates the thermal decomposition of ferromanganoan dolomite using DTA and X-ray powder analysis under four different atmospheres including static air.

In a $CO_2$ flow of 100 ml $min^{-1}$, it decomposes in three steps

FeMn-dolomite $\rightarrow CaCO_3 + (Fe, Mn)_3O_4 + MgO$

$\rightarrow CaCO_3 + CaMnO_3 + CaFe_2O_4 + MgO$

$\rightarrow CaMnO_3 + CaFe_2O_4 + MgO + CaO$

However, in a mixed gas flow of $CO_2$ at 95 ml $min^{-1}$ and CO at 5 ml $min^{-1}$, it decomposes in two steps

FeMn-dolomite $\rightarrow CaCO_3 + (Mg, Mn)\underline{O} + Fe_2O_3$

$\rightarrow (Ca, Mn)O + (Mg, Mn)\overline{O} + Ca_2MgFe_2O_6$

In a mixed gas flow of $CO_2$ at 50 ml $min^{-1}$ and CO at 50 ml $min^{-1}$, the decomposition proceeds in two steps

FeMn-dolomite $\rightarrow CaCO_3 + (Mg, Mn, Fe)\underline{O}$

$\rightarrow (Ca, Mn, Fe)O + (Mg, Mn, Fe)\overline{O}$

It has been found that when the $O_2$ partial pressure in the atmosphere is low enough to keep Mn and Fe in a bivalent state, dolomite group minerals bearing Mn and Fe decompose in a similar manner to dolomite itself.

## INTRODUCTION

As a part of the thermoanalytical study of dolomite and related minerals [1,2], the authors have already reported the thermal decomposition of magnesian kutnahorite containing $Mn^{2+}$ as a substituent for $Mg^{2+}$ in the dolomite structure [3]. However, $Fe^{2+}$ is the more common substituent for $Mg^{2+}$ in naturally occurring dolomite. Therefore, in the present study, ferromanganoan dolomite was selected in order to examine how substituent $Fe^{2+}$ as well as $Mn^{2+}$ affect the thermal decomposition of dolomite itself.

Studies of the thermal decomposition of Mn-bearing dolomite group

0040-6031/83/$03.00 

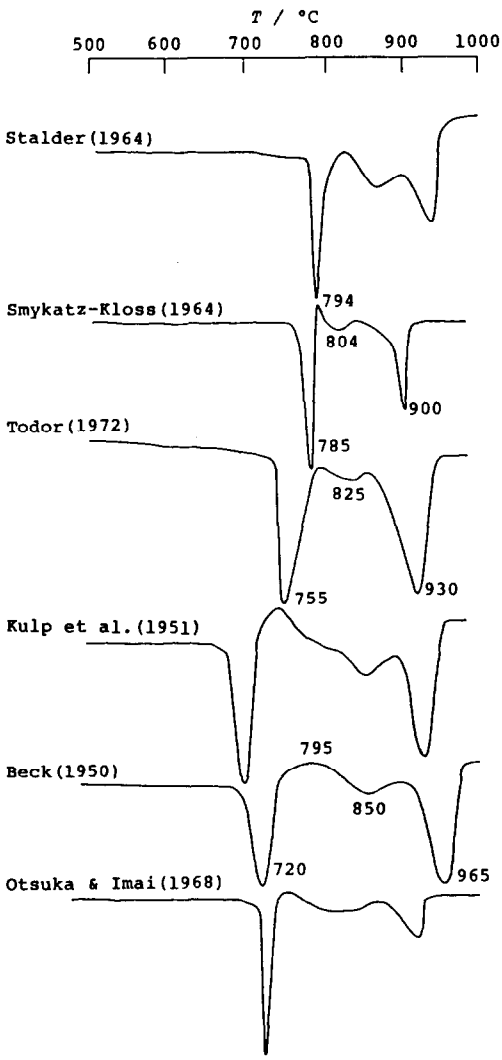


Fig. 1. Some DTA curves of ferroan dolomite published previously.

minerals are scarce because of their less common occurrence. On the other hand, as the minerals belonging to the dolomite–ankerite series are relatively common in nature, their thermal decompositions have been studied extensively.

Figure 1 shows the DTA curves of ferroan dolomite obtained by several workers [4–9]. All these curves were obtained in static air atmospheres using several hundred mg of the samples. They show two large endotherms which are accompanied by a small broad endothermic peak between them. Some of the curves have a small exothermic hump following the first endotherm. Although these curves have similar patterns, they are interpreted quite differently by the workers concerned.

Beck [8] and Smykatz-Kloss [5] attributed the first peak to the decomposition of the $FeCO_3$ part, the second to the $MgCO_3$ part and the third to the $CaCO_3$ part of ferroan dolomite: they attributed the exotherm to the oxidation of $Fe^{2+}$ to form $Fe_3O_4$. Beck [8] confirmed CaO and $MgO \cdot Fe_2O_3$ as the final products. To the contrary, Todor [6] attributed the first peak to the decomposition of the $MgCO_3$ part and the second to the $FeCO_3$. Kulp et al. [7] explained that the first peak was due to the decomposition of the $CO_3^{2-}$ most closely associated with the Mg sites to form $CaCO_3$, MgO and maghemite ($\gamma$-$Fe_2O_3$), the second to the formation of $Fe_2O_3 \cdot CaCO_3$, and the third to the decomposition of $Fe_2O_3 \cdot CaCO_3$ forming $CaO \cdot Fe_2O_3$. Otsuka and Imai [9] inferred that the second peak was due to the reaction of $CaCO_3$ and $Fe_2O_3$ to form $2CaO \cdot Fe_2O_3$ and $CaO \cdot Fe_2O_3$, and that the third peak was due to the decomposition of the unreacted $CaCO_3$. Stalder [4] concluded that the first peak was due to the formation of $CaCO_3$ by cation diffusion in the lattice releasing the $CO_2$ bonded to Fe, Mg and Mn, with the formation of $Fe_3O_4$ and MgO. The second and third endotherms show essentially a single endothermic reaction due to the decomposition of $CaCO_3$. This reaction, however, was apparently separated by various exothermic reactions due to the formation of $Fe_2O_3$ or $2CaO \cdot Fe_2O_3$. He recognized 2 $CaO \cdot MgO \cdot Fe_2O_3$ as well as CaO and $2CaO \cdot Fe_2O_3$ as the final products.

## MATERIAL

Ferromanganoan dolomite from the Budo mine, Niigata Prefecture, Japan was used in this study. Chemical composition (wt.%) and cation mole ratio (mole%) were obtained by EPMA (apparatus, JEOL JXA-50A). Correction was made by the method of Bence and Albee (Table 1). The structural formula was calculated assuming an oxidation number of 6, $Ca_{1.015}(Mg_{0.515}Fe_{0.225}Mn_{0.245})(CO_3)_2$. X-Ray powder analysis confirmed that this material was free from other minerals. The lattice parameters obtained using silicon (99.9999%) as an internal standard were $a = 4.8310 \pm 0.0006$ Å and $c =$

TABLE 1

Chemical composition (wt.%) and cation mole ratio (mole%) of FeMn-dolomite

| Chemical composition | wt.% | Cation mole ratio | mole% |
|---|---|---|---|
| CaO | 27.74 | $CaCO_3$ | 50.77 |
| MgO | 10.10 | $MgCO_3$ | 25.72 |
| FeO | 7.89 | $FeCO_3$ | 11.27 |
| MnO | 8.46 | $MnCO_3$ | 12.24 |
| $CO_2$ | 42.88 | | |
| Total | 97.07 | | |

16.148 ± 0.005 Å. The ordered reflections, (015) and (309) observed in the powder pattern, show that this material belongs to dolomite group of $R\bar{3}$ symmetry. Ferromanganoan dolomite is abbreviated to FeMn-dolomite in this paper.

## EXPERIMENTAL

FeMn-dolomite was ground in an agate mortar and fractions finer than 325 mesh (43 μm) for experiment were obtained by sieving.

### *DTA measurement*

DTA curves were recorded by a Shinku Riko ULVAC DT-1500H incorporating a Pt–PtRh13% thermocouple, Pt micro sample pan and using calcined alumina as a reference material, under the given conditions: sample weight, 5.0 mg; programmed heating rate, 10°C $min^{-1}$; DTA sensitivity, ±50μV. Measurements were performed in atmospheres of

(1) static air, (2) $CO_2$ flow at 100 ml $min^{-1}$, (3) a mixed gas flow of $CO_2$ at 95 ml $min^{-1}$ and CO at 5 ml $min^{-1}$, and (4) a mixed gas flow of $CO_2$ at 50 ml $min^{-1}$ and CO at 50 ml $min^{-1}$. These atmospheres are abbreviated as air, $CO_2$, CO 5% and CO 50%, respectively.

### *X-Ray powder analysis*

The phase identification of the reaction products were made by X-ray powder analysis using a Rigaku Geigerflex 2001, under the given conditions: Ni-filtered Cu$K_\alpha$ radiation ($\lambda$ = 1.5418 Å), 40 kV, 20 mA, time constant 2 s, scanning speed 0.5° $min^{-1}$, divergence slit 1°, receiving slit 0.3 mm and scattering slit 1°.

After being heated to a certain temperature as determined by the DTA curves, the samples were rapidly cooled to room temperautre by removing the furnace, and then subjected to X-ray analysis.

## RESULTS

### *DTA curves of FeMn-dolomite*

Figure 2 shows the DTA curves of FeMn-dolomite in the four atmospheres. The DTA curve obtained in air, (A), has a single asymmetric endotherm, showing a remarkable difference from any other curves in Fig. 1. This may be attributed to the effect of a self-generating $CO_2$ atmosphere as in the decompositions of dolomite and magnesian kutnahorite [1,3].

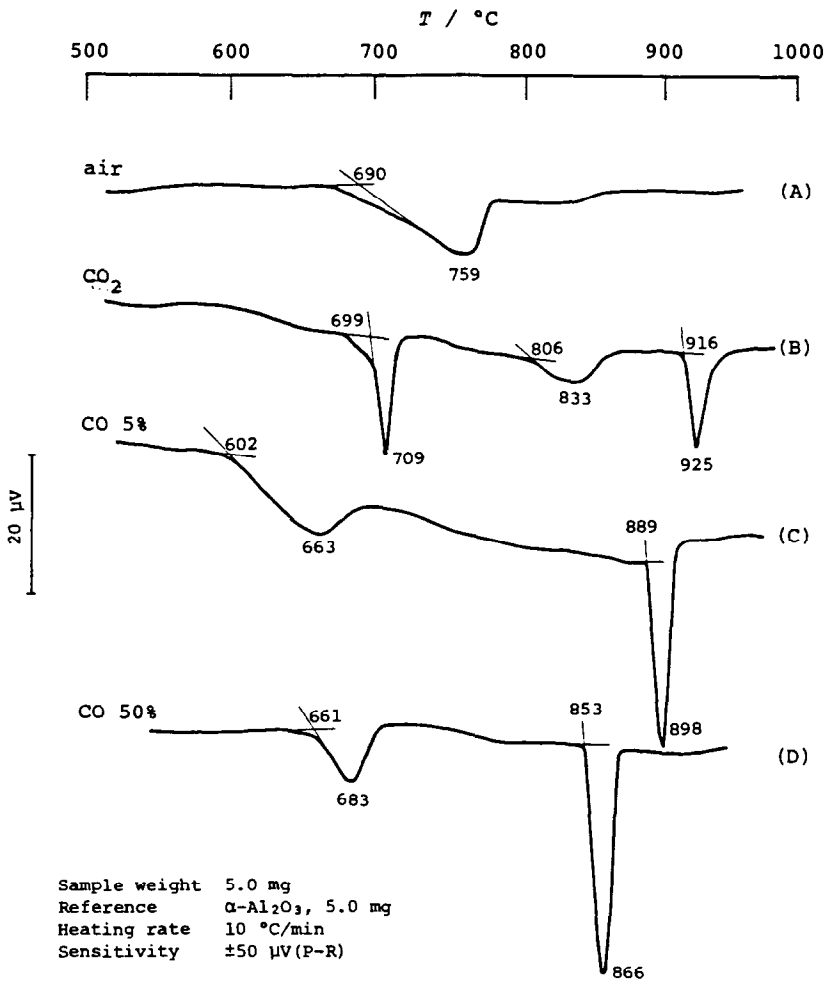


Fig. 2. DTA curves of FeMn-dolomite under the four atmospheres.

The DTA curve in $CO_2$, (B), shows three discrete endotherms which are accompanied by a very weak exothermic hump immediately after the first peak. Curve (B) is very similar to those in Fig. 1 obtained in static air. The cooling DTA curve recorded at a programmed rate of 10°C $min^{-1}$ after the completion of the decomposition showed that only the third peak gave a reverse exotherm.

The DTA curves in CO 5%, (C), and CO 50%, (D), showed two endotherms which are like the two step decomposition of dolomite. In CO 5%, the first peak shows a fairly broad and asymmetric shape starting at about 600°C, while it shows a symmetric shape like an isosceles triangle beginning at about 660°C in CO 50%. The DTA cooling curves in CO 5% and CO 50%

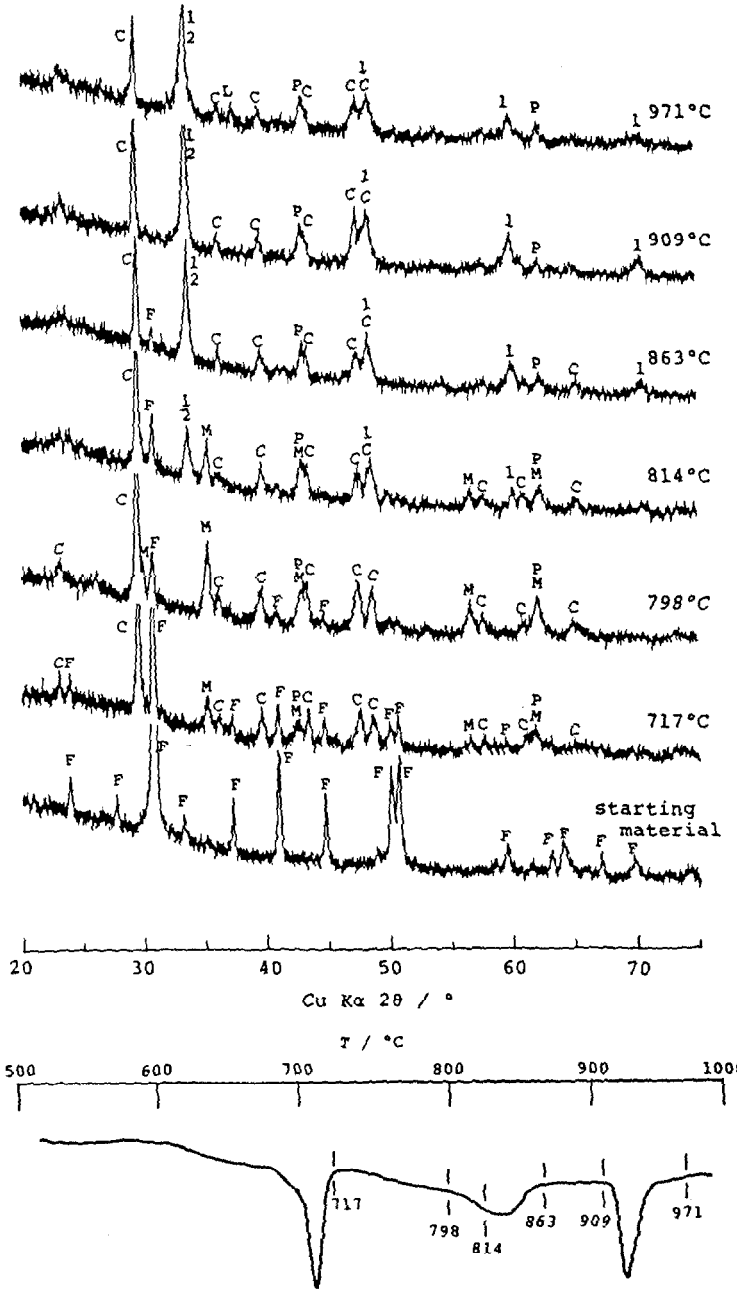


Fig. 3. X-Ray diffraction patterns of the thermal decomposition products of FeMn-dolomite in $CO_2$. F, FeMn-dolomite; C, $CaCO_3$; M, $(Fe, Mn)_3O_4$; P, MgO; 1, $CaMnO_3$; 2, $CaFe_2O_4$; L, CaO. Each temperature, to which the sample was heated, is indicated beneath the DTA curve in the lower part.

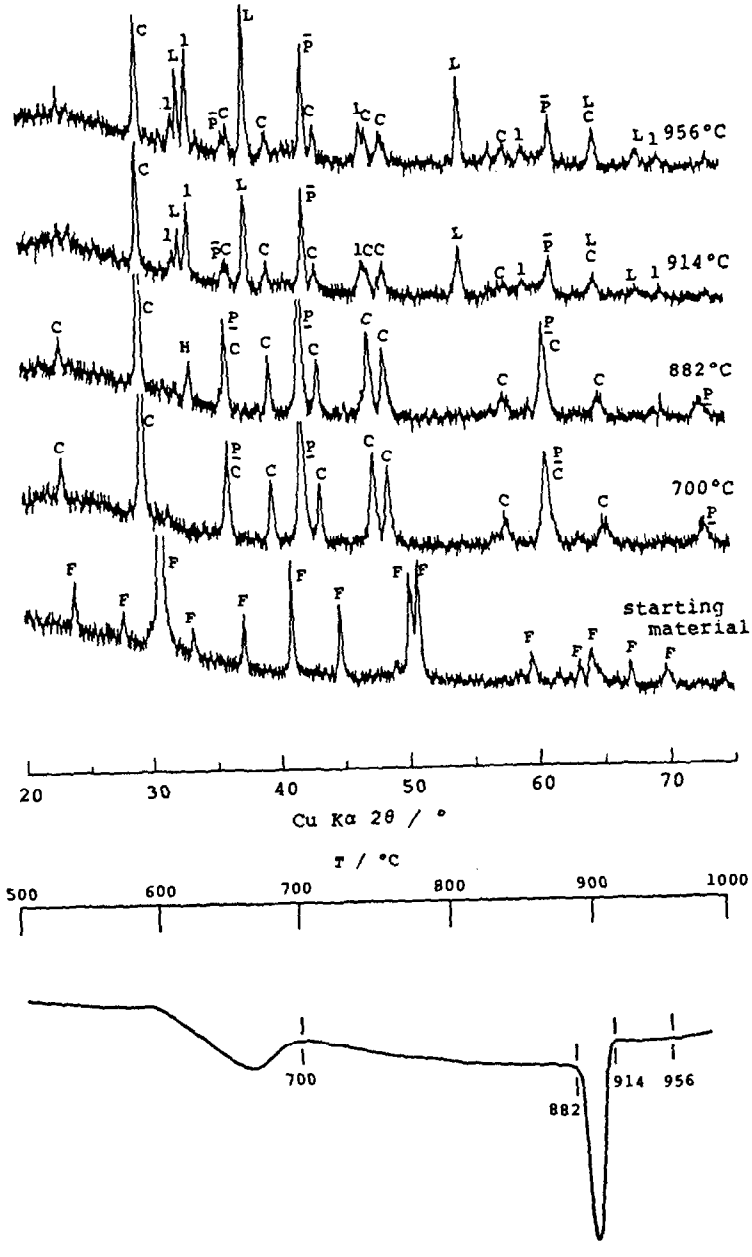


Fig. 4. X-Ray diffraction patterns of the thermal decomposition products of FeMn-dolomite in CO 5%. F, FeMn-dolomite; C, $CaCO_3$; $\underline{P}$, (Mg, M)$\underline{O}$; $\bar{P}$, (Mg, M)$\bar{O}$; H, $Fe_2O_3$; L, (Ca, M)O; 1, $Ca_2MgFe_2O_6$ (M is Mn and/or Fe). Each temperature, to which the sample was heated, is indicated beneath the DTA curve in the lower part.

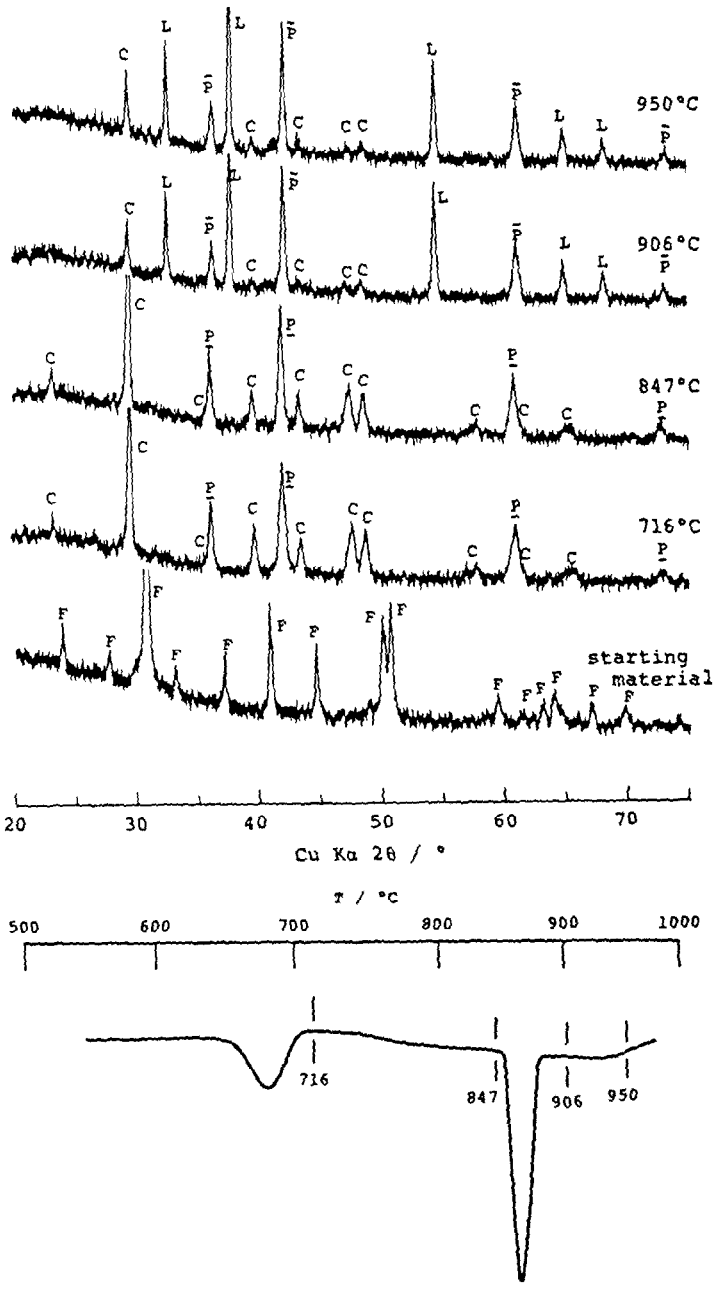


Fig. 5. X-Ray diffraction patterns of the thermal decomposition products of FeMn-dolomite in CO 50%. F, FeMn-dolomite; C, $CaCO_3$; $\underline{P}$, (Mg, M)$\underline{O}$; $\overline{P}$, (Mg, M)$\overline{O}$; L, (Ca, M)O (M is Mn and/or Fe). Each temperature, to which the sample was heated, is indicated beneath the DTA curve in the lower part.

show the exotherms corresponding to the second endotherms. The exotherms are, however, extremely small compared with that of dolomite.

*Identification of products*

The products in $CO_2$, CO 5% and CO 50% were observed by X-ray powder analysis. These results are shown in Figs. 3–5. Each temperature, to which the sample was heated, is indicated beneath the DTA curves in the lower parts of these figures. In the upper parts the X-ray powder patterns of the products obtained by heating are reproduced. Further, the products identified are listed in Tables 2–4.

In $CO_2$ (Fig. 3), at 717°C, FeMn-dolomite and the $CaCO_3$ produced were observed, and weak reflections, presumably due to (Fe, Mn)$_3O_4$ solid solution [10], were detected. Because of the overlapping of the reflections of MgO with those of (Fe, Mn)$_3O_4$, the identification of MgO was difficult. However, MgO was expected to exist since the content of Mg in the original sample is twice as much as that of Fe and Mn. At 814°C, a new phase, $CaMnO_3$, was confirmed. As shown in Table 1, Fe and Mn were contained in nearly equal amounts in the original sample, so $CaFe_2O_4$ was also formed.

TABLE 2

Thermal decomposition products of FeMn-dolomite in $CO_2$

| Temperature, $T$ (°C) | Products observed by powder X-ray analysis |
|---|---|
| 717 | $CaCO_3$, FeMn-dolomite, (Fe, Mn)$_3O_4$, MgO |
| 798 | $CaCO_3$, (Fe,Mn)$_3O_4$, MgO, FeMn-dolomite |
| 814 | $CaCO_3$, $CaMnO_3$, $CaFe_2O_4$, (Fe, Mn)$_3O_4$, MgO, FeMn-dolomite |
| 863 | $CaMnO_3$, $CaFe_2O_4$, $CaCO_3$, MgO, FeMn-dolomite |
| 909 | $CaMnO_3$, $CaFe_2O_4$, $CaCO_3$, MgO |
| 971 | $CaMnO_3$, $CaFe_2O_4$, MgO, CaO, $CaCO_3$ |

TABLE 3

Thermal decomposition products of FeMn-dolomite in CO 5%

| Temperature, $T$ (°C) | Products observed by powder X-ray analysis |
|---|---|
| 700 | $CaCO_3$, (Mg, M)O |
| 882 | $CaCO_3$, (Mg, M)O, $Fe_2O_3$ |
| 914 | (Ca, M)O, (Mg, M)O, $Ca_2MgFe_2O_6$, $CaCO_3$ |
| 956 | (Ca, M)O, (Mg, M)O, $Ca_2MgFe_2O_6$, $CaCO_3$ |

M = Mn and/or Fe

TABLE 4

Thermal decomposition products of FeMn-dolomite in CO 50%

| Temperature, $T$ (°C) | Products observed by powder X-ray analysis |
|---|---|
| 716 | $CaCO_3$, (Mg, M)$\underline{O}$ |
| 847 | $CaCO_3$, (Mg, M)$\underline{O}$ |
| 906 | (Ca, M)O, (Mg, M)$\overline{O}$, $CaCO_3$ |
| 950 | (Ca, M)O, (Mg, M)$\overline{O}$, $CaCO_3$ |

M = Mn and/or Fe

probably together with $CaMnO_3$. However, no other reflections of $CaFe_2O_4$ other than the most intense one overlapping with that of $CaMnO_3$, were recognized. At 863°C, with the decrease of the amount of $CaCO_3$, (Fe, Mn)$_3O_4$ disappeared, while the amount of $CaMnO_3$ and $CaFe_2O_4$ increased. At 909°C, FeMn-dolomite disappeared completely. At 971°C, the reflections of $CaCO_3$ were remarkably weakened, while a new phase, CaO, appeared.

In CO 5% (Fig. 4), at 700°C, FeMn-dolomite disappeared, while $CaCO_3$ and periclase solid solution (Mg, M)$\underline{O}$ were detected. M represents $Mn^{2+}$ and/or $Fe^{2+}$ incorporated in the structure. At 882°C, a new reflection, probably the most intense peak of $\alpha$-$Fe_2O_3$, appeared. At 914°C, with the decrease of the amount of $CaCO_3$, periclase solid solution having a different composition, (Mg, M)$\overline{O}$, from (Mg, M)$\underline{O}$, lime solid solution, (Ca, M)O, and a new phase considered as $Ca_2MgFe_2O_6$ (ASTM 2-0938), were found. The periclase solid solution decreased its lattice parameter from (Mg, M)$\underline{O}$ to (Mg, M)$\overline{O}$. At 956°C, the reflections of $CaCO_3$ decreased, while the reflections of the other products increased.

In CO 50% (Fig. 5), at 716°C, $CaCO_3$ and periclase solid solution (Mg, M)$\underline{O}$ were observed. No other products were detected by heating to 847°C. At 906°C, periclase solid solution, (Mg, M)$\overline{O}$, and lime solid solution, (Ca, M)O, were detected with a trace amount of $CaCO_3$. As in the case of CO 5%, the periclase solid solution decreased its lattice parameter from (Mg, M)$\underline{O}$ to (Mg, M)$\overline{O}$ in CO 50%. The behaviours at 906°C were unchanged even at 956°C.

## DISCUSSION

### *Decomposition in $CO_2$*

Figure 6 shows the three-step decomposition of FeMn-dolomite in $CO_2$. At the first step, the original FeMn-dolomite decomposes into $CaCO_3$, (Fe, Mn)$_3O_4$ solid solution and MgO, releasing $CO_2$ of the corresponding amount

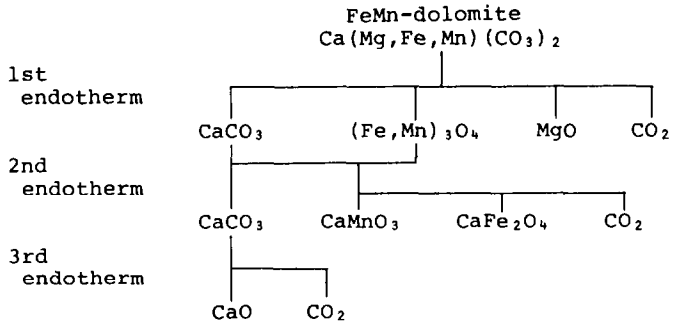


Fig. 6. Thermal decomposition process of FeMn-dolomite in $CO_2$.

to Mg, Fe and Mn. At the second step, $(Fe, Mn)_3O_4$ reacts with $CaCO_3$ to produce $CaMnO_3$ and $CaFe_2O_4$, releasing $CO_2$. At the third step, as confirmed by the reverse exotherm on cooling, the residual $CaCO_3$ decomposes.

The similarity of curve (B) in Fig. 2 to those in Fig. 1 suggests that the latter curves were obtained under the self-generating $CO_2$ atmospheres reaching up to almost 1 atm in the vicinity of the samples. The explanations of the DTA curves by previous workers, however, are different from the present interpretations.

Though Beck [8], Smykatz-Kloss [5] and Todor [6] considered that the partial decompositions of the three component carbonates ($FeCO_3$, $MgCO_3$ and $CaCO_3$) corresponded to the three endotherms, their interpretations cannot explain the formation of Ca-Fe oxides or Ca-Mn oxides at the second step. On curve (B) in Fig. 2, the second and third peaks are clearly separated and the base line between them is stable, so Stalder's interpretation [4] that the two peaks essentially form a single endothermic peak due to the decomposition of $CaCO_3$ cannot be supported. Thus, the interpretations of the previous workers cannot explain the present results.

*Decomposition in CO 5%*

FeMn-dolomite decomposes in two steps in CO 5% (Fig. 7). At the first step, the original FeMn-dolomite decomposes into $CaCO_3$ and oxides of Mg,

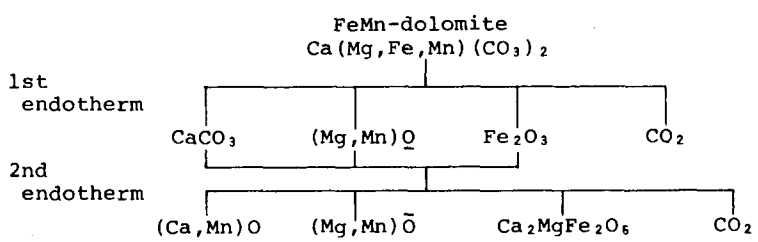


Fig. 7. Thermal decomposition process of FeMn-dolomite in CO 5%.

Mn and Fe, releasing $CO_2$ of the corresponding amount to Mg, Fe and Mn. Of the oxide products, only periclase solid solution, (Mg, M)$\underline{O}$, is observed at 700°C. $Fe_2O_3$, which is detected at 882°C, has probably been crystallized gradually by further heating above 700°C. At the second step, $CaCO_3$ reacts with (Mg, M)$\underline{O}$ and $Fe_2O_3$, releasing $CO_2$ to produce lime solid solution, (Ca, M)O, and periclase solid solution, (Mg, M)$\overline{O}$, which have a different chemical composition from (Mg, M)$\underline{O}$ and $Ca_2MgFe_2O_6$.

As stated previously, $Fe_2O_3$ appears at a higher temperature (882°C) than the temperature (700°C) at which the first step decomposition terminates. It is not expected that $Fe_2O_3$ contains Mn, because, as shown below, Mn remains bivalent in CO 5%. The lattice parameter, $a = 4.301$ Å, and the intensity of each diffraction of (Mg, M)$\underline{O}$ remained unchanged between 700 and 882°C. This suggests that the FeO component did not leave the (Mg, M)$\underline{O}$ gradually, but was separated completely from (Mg, M)$\underline{O}$ at the time of the first decomposition step. If so, (Mg, Mn)$\underline{O}$ would be a more appropriate expression of periclase solid solution, (Mg, M)$\underline{O}$, because all the Fe was probably removed from this phase during the first decomposition step. On this assumption, the Mg/Mn ratio in (Mg, Mn)$\underline{O}$ can be estimated as 66.2/33.8 based on the observed value, $a = 4.301$ Å, from the relation of chemical composition with lattice parameter in the MgO–MnO system [11]. On the other hand, the Mg/Mn ratio in the original FeMn-dolomite is 67.8/32.2 (Table 1), which agrees fairly well with the value obtained from the lattice parameter. This agreement strongly supports the expression (Mg, Mn)$\underline{O}$. Accordingly, in the case of (Mg, M)$\overline{O}$ and (Ca, M)O, (Mg, Mn)$\overline{O}$ and (Ca, Mn)O are more appropriate expressions.

Moreover, the absence of any exothermic deflection between the two endothermic peaks suggests that the oxidation of $Fe^{2+}$ to trivalent iron has proceeded already during the first decomposition step forming a certain X-ray amorphous $Fe^{3+}$ oxide, which crystallized as $Fe_2O_3$ on further heating.

Therefore, the first decomposition step consists of: the decomposition of FeMn-dolomite, the formation of $CaCO_3$ and (Mg, Mn)$\underline{O}$, the separation and oxidation of the FeO component, and the successive gradual crystallization of $Fe_2O_3$. The decrease in the lattice parameter of periclase solid solution from (Mg, Mn)$\underline{O}$ to (Mg, Mn)$\overline{O}$ at the second decomposition step may be explained by re-distribution of Mn between periclase and lime solid solutions as in the case of magnesian kutnahorite. However, since Mn probably substitutes for Ca and/or Mg in $Ca_2MgFe_2O_6$ too, the redistribution process is more complicated in this case.

*Decomposition in CO 50%*

Figure 8 shows the decomposition process of FeMn-dolomite in CO 50%. In this atmosphere, as in CO 5%, it decomposes in two steps. At the first step, FeMn-dolomite decomposes into $CaCO_3$ and periclase solid solution,

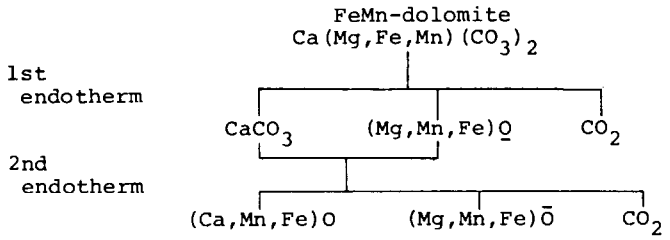


Fig. 8. Thermal decomposition process of FeMn-dolomite in CO 50%.

(Mg, M)O, releasing $CO_2$ of the corresponding amount to Mg, Mn and Fe. At the second step, $CaCO_3$ reacts with (Mg, M)O to produce lime solid solution, (Ca, M)O, and periclase solid solution, (Mg, M)$\overline{O}$, which has a different chemical composition from (Mg, M)O. Owing to the re-distribution of Fe and Mn between (Mg, M)O and CaO, which is produced from $CaCO_3$ at this step, the lattice parameters of (Ca, M)O and (Mg, M)$\overline{O}$ become smaller than those of CaO and (Mg, M)O.

The lattice parameter of each solid solution is determined using its (200) diffraction: (Mg, M)$\overline{O}$, 4.283 Å; (Ca, M)O, 4.752 Å.

From the following discussions, it is deduced that the equilibrium re-distribution of Fe and Mn between (Mg, M)$\overline{O}$ and (Ca, M)O is achieved at the second decomposition step.

At first, it is assumed that all the Mg, Mn and Fe in the original FeMn-dolomite have participated in the formation of the solid solutions. However, the amount of Ca being incorporated in the solid solution is unknown because of the partial re-carbonation of CaO to $CaCO_3$. As the CaO–MgO system scarcely forms solid solution series below 1000°C [12], (Ca, Mg)O and (Ca, Mg, M)O are not considered in the succeeding discussion. Accordingly, the solid solutions produced are regarded as (Mg, Mn, Fe)$\overline{O}$ and (Ca, Mn, Fe)O.

Next, it is necessary to know the relations between composition and activity and between composition and lattice parameter of solid solutions of the ternary systems CaO–MnO–FeO and MgO–MnO–FeO. However, there are no available data except composition vs. activity relations in the CaO–MnO–FeO system [13], which is hardly used in the numerical analysis because of the graphical representation using equi-activity contours in a triangle diagram. On the other hand, composition vs. activity relations are reported for the binary systems, CaO–MnO [13], FeO–MgO [14], MgO–MnO [15], MnO–FeO [16] and FeO–CaO [17]. Also, the relation between composition and lattice parameter is available for the FeO–MgO, MnO–FeO, CaO–MnO and MgO–MnO systems [11]. Therefore, it will be reasonable to represent a ternary system using a model that is constructed from the three binary systems included in the ternary system.

Using the asymmetric solution model [18], the excess Gibbs energy of the

binary system 1–2, $G_{12}^{ex}$, is expressed by

$$G_{12}^{ex} = x_1 x_2 (x_1 W_{12} + x_2 W_{21}) \tag{1}$$

where $x_i$ is the mole fraction of component $i$, $W_{12}$ and $W_{21}$ are the parameters representing the characteristics of the 1–2 binary system. The general thermodynamic expression for $G_{12}^{ex}$ is

$$G_{12}^{ex} = x_1 RT \ln \gamma_1 + x_2 RT \ln \gamma_2 \tag{2}$$

$$\gamma_i = \frac{a_i}{x_i} \tag{3}$$

where $\gamma_i$ is the activity coefficient and $a_i$ is the activity of component $i$. Because available data for the temperature region of this experiment (500–1000°C) are lacking, substituting the previous data estimated at about 1100°C [13–17] into these equations, the parameters $W_{12}$ and $W_{21}$ are estimated by the least-squares method as in Table 5. Using the six parameters of three binary systems, 1–2, 2–3 and 3–1, the excess Gibbs energy of the ternary system 1–2–3 is expressed according to Thompson [18]

$$G_{123}^{ex} = x_1 x_2 (x_1 W_{12} + x_2 W_{21}) + x_2 x_3 (x_2 W_{23} + x_3 W_{32}) + x_3 x_1 (x_3 W_{31} + x_1 W_{13}) \tag{4}$$

$$RT \ln \gamma_1 = G_{123}^{ex} - x_2 \left( \frac{\partial G_{123}^{ex}}{\partial x_2} \right)_{TP} - x_3 \left( \frac{\partial G_{123}^{ex}}{\partial x_3} \right)_{TP} \tag{5}$$

Since eqn. (5) holds generally in the ternary system, the activity coefficient of component 1 is obtained by substitution of eqn. (4) into eqn. (5)

$$\begin{aligned} RT \ln \gamma_1 = {} & x_2^3 (2W_{21} - 2W_{12}) + x_3^3 (2W_{31} - 2W_{13}) \\ & + x_2^2 x_3 (-4W_{12} + 2W_{21} - 2W_{13} - 2W_{23}) \\ & + x_2 x_3^2 (-4W_{13} + 2W_{31} - 2W_{12} - 2W_{32}) \\ & + x_2^2 (2W_{12} - W_{21}) + x_3^2 (2W_{13} - W_{31}) \\ & + x_2 x_3 (2W_{12} + 2W_{13}) \end{aligned} \tag{6}$$

TABLE 5

Parameters $W$ of the binary asymmetric solution model, eqn. (1)

| System $i-j$ | $W_{ij}$ | $W_{ji}$ |
|---|---|---|
| CaO–MnO | 3555.60 | 2906.48 |
| FeO–MgO | 3291.09 | 2642.90 |
| MgO–MnO | 3801.08 | 4684.86 |
| MnO–FeO | 732.69 | 1625.98 |
| FeO–CaO | 3865.73 | 7884.42 |

Expressions for components 2 and 3 can be obtained by permuting the subscripts in the cyclic order of 1→2→3.

The equilibrium condition of the re-distribution of Mn and Fe between (Ca, M)O and (Mg, M)$\overline{O}$ can be expressed by the Nernst distribution law applied to MnO and FeO components independently.

$$\mu^{L}_{MnO} = \mu^{P}_{MnO} \tag{7}$$

$$\mu^{L}_{FeO} = \mu^{P}_{FeO} \tag{8}$$

where P and L represent the periclase and lime phases, respectively. As a common standard state is adopted in both sides of each equation, eqns. (7) and (8) are simplified using only the activity terms

$$a^{L}_{MnO} = a^{P}_{MnO} \tag{9}$$

$$a^{L}_{FeO} = a^{P}_{FeO} \tag{10}$$

These conditions are represented using eqns. (3) and (6) as given by

$$\begin{aligned}
&RT \ln x^{L}_{MnO} + x^{L^3}_{FeO}(2W_{FeMn} - 2W_{MnFe}) + x^{L^3}_{CaO}(2W_{CaMn} - 2W_{MnCa}) \\
&\quad + x^{L^2}_{FeO}x^{L}_{CaO}(-4W_{MnFe} + 2W_{FeMn} - 2W_{MnCa} - 2W_{FeCa}) \\
&\quad + x^{L}_{FeO}x^{L^2}_{CaO}(-4W_{MnCa} + 2W_{CaMn} - 2W_{MnFe} - 2W_{CaFe}) \\
&\quad + x^{L^2}_{FeO}(2W_{MnFe} - W_{FeMn}) + x^{L^2}_{CaO}(2W_{MnCa} - W_{CaMn}) \\
&\quad + x^{L}_{FeO}x^{L}_{CaO}(2W_{MnFe} + 2W_{MnCa}) \\
&= RT \ln x^{P}_{MnO} + x^{P^3}_{FeO}(2W_{FeMn} - 2W_{MnFe}) + x^{P^3}_{MgO}(2W_{MgMn} - 2W_{MnMg}) \\
&\quad + x^{P^2}_{FeO}x^{P}_{MgO}(-4W_{MnFe} + 2W_{FeMn} - 2W_{MnMg} - 2W_{FeMg}) \\
&\quad + x^{P}_{FeO}x^{P^2}_{MgO}(-4W_{MnMg} + 2W_{MgMn} - 2W_{MnFe} - 2W_{MgFe}) \\
&\quad + x^{P^2}_{FeO}(2W_{MnFe} - W_{FeMn}) + x^{P^2}_{MgO}(2W_{MnMg} - W_{MgMn}) \\
&\quad + x^{P}_{FeO}x^{P}_{MgO}(2W_{MnFe} + 2W_{MnMg})
\end{aligned} \tag{11}$$

and

$$\begin{aligned}
&RT \ln x^{L}_{FeO} + x^{L^3}_{CaO}(2W_{CaFe} - 2W_{FeCa}) + x^{L^3}_{MnO}(2W_{MnFe} - 2W_{FeMn}) \\
&\quad + x^{L^2}_{CaO}x^{L}_{MnO}(-4W_{FeCa} + 2W_{CaFe} - 2W_{FeMn} - 2W_{CaMn}) \\
&\quad + x^{L}_{CaO}x^{L^2}_{MnO}(-4W_{FeMn} + 2W_{MnFe} - 2W_{FeCa} - 2W_{MnCa}) \\
&\quad + x^{L^2}_{CaO}(2W_{FeCa} - W_{CaFe}) + x^{L^2}_{MnO}(2W_{FeMn} - W_{MnFe}) \\
&\quad + x^{L}_{CaO}x^{L}_{MnO}(2W_{FeCa} + 2W_{FeMn}) \\
&= RT \ln x^{P}_{FeO} + x^{P^3}_{MgO}(2W_{MgFe} - 2W_{FeMg}) + x^{P^3}_{MnO}(2W_{MnFe} - 2W_{FeMn}) \\
&\quad + x^{P^2}_{MgO}x^{P}_{MnO}(-4W_{FeMg} + 2W_{MgFe} - 2W_{FeMn} - 2W_{MgMn})
\end{aligned}$$

$$+x^{P}_{MgO}x^{P^2}_{MnO}(-4W_{FeMn}+2W_{MnFe}-2W_{FeMg}-2W_{MnMg})$$
$$+x^{P^2}_{MgO}(2W_{FeMg}-W_{MgFe})+x^{P^2}_{MnO}(2W_{FeMn}-W_{MnFe})$$
$$+x^{P}_{MgO}x^{P}_{MnO}(2W_{FeMg}+2W_{FeMn}) \quad (12)$$

When the chemical composition of a solid solution is estimated from its lattice parameter, the Vegard law is commonly applied. However, it is found that lattice parameters of MO-type solid solutions are more or less larger than those approximated by the Vegard law which assumes a linear relation between the composition and the lattice parameter [11]. In order to improve the approximation, a correction term of $x_1x_2B_{12}$, which is the analogous form of the excess Gibbs energy of a regular solution model, is to be added to the Vegard law. Then, the lattice parameter $A$ of a solid solution is represented by

$$A = x_1A_1 + x_2A_2 + x_1x_2B_{12} \quad (13)$$

where $A_i$ is the lattice parameter of the end member of component $i$, $B_{12}$ is the interaction parameter of the lattice parameter of the system 1–2. The first two terms of the right side show the Vegard law. Substituting the chemical compositions and corresponding lattice parameters of solid solutions [11] into eqn. (13), the parameter $B$ of binary systems is estimated by the least-squares method as in Table 6. The solubility of the FeO component in CaO is so limited by the miscibility gap [17] that the value of $B$ for the CaO–FeO system is assumed to be 0. Using three parameters of the binary systems of 1–2, 2–3 and 3–1, the lattice parameter, $A$, of a solid solution of a ternary system of 1–2–3 may, after taking eqn. (4) into account, be represented by

$$A = x_1A_1 + x_2A_2 + x_3A_3 + x_1x_2B_{12} + x_2x_3B_{23} + x_3x_1B_{31} \quad (14)$$

Using this expression, the lattice parameters of (Ca, M)O and (Mg, M)$\overline{O}$, $A^L$ and $A^P$, are given by

$$A^L = x^L_{CaO}A_{CaO} + x^L_{MnO}A_{MnO} + x^L_{FeO}A_{FeO}$$

TABLE 6

Parameters $B$ of the binary lattice parameter, eqn. (13)

| System $i-j$ | $B_{ij}$ |
|---|---|
| CaO–MnO | 0.00320 |
| FeO–MgO | 0.06357 |
| MgO–MnO | 0.05489 |
| MnO–FeO | 0.02423 |
| FeO–CaO | 0 |

$$+x^{L}_{CaO}x^{L}_{MnO}B_{CaMn}+x^{L}_{MnO}x^{L}_{FeO}B_{MnFe}$$
$$+x^{L}_{FeO}x^{L}_{CaO}B_{FeCa} \quad (15)$$

and,

$$A^{P}=x^{P}_{MgO}A_{MgO}+x^{P}_{MnO}A_{MnO}+x^{P}_{FeO}A_{FeO}$$
$$+x^{P}_{MgO}x^{P}_{MnO}B_{MgMn}+x^{P}_{MnO}x^{P}_{FeO}B_{MnFe}$$
$$+x^{P}_{FeO}x^{P}_{MgO}B_{FeMg} \quad (16)$$

The following equations are held by the definition of mole fraction

$$x^{L}_{CaO}+x^{L}_{MnO}+x^{L}_{FeO}=1 \quad (17)$$

$$x^{P}_{MgO}+x^{P}_{MnO}+x^{P}_{FeO}=1 \quad (18)$$

If the equilibrium re-distribution of Mn and Fe between (Ca, M)O and (Mg, M)$\overline{O}$ is achieved, the chemical compositions of both phases can be estimated by solving the simultaneous eqns. (11) and (12) representing the equilibrium condition, eqns. (15) and (16) representing the lattice parameters, and eqns. (17) and (18), regarding $x^{L}_{CaO}$, $x^{L}_{MnO}$, $x^{L}_{FeO}$, $x^{P}_{MgO}$, $x^{P}_{MnO}$ and $x^{P}_{FeO}$ as variables.

These are solved numerically substituting the observed lattice parameters in eqns. (15) and (16): (Mg, M)$\overline{O}$, $(Mg_{0.615}Mn_{0.154}Fe_{0.231})O$; (Ca, M)O, $(Ca_{0.860}Mn_{0.103}Fe_{0.037})O$. The chemical composition of (Mg, M)$\overline{O}$ will be represented by $(Mg_{25.72}Mn_{6.44}Fe_{9.66})O_{41.82}$ based on the $MgCO_3$ mole% (25.72) in FeMn-dolomite in Table 1. The amounts of Mn and Fe included in (Mg, M)$\overline{O}$ are estimated as 6.44 and 9.66. Therefore, the amount of Mn included in (Ca, M)O is 5.80 which is the remainder of the Mn content (6.44) in (Mg, M)$\overline{O}$ from the $MnCO_3$ mole% (12.24) in FeMn-dolomite. Then, the chemical composition of (Ca, M)O can be expressed as $(Ca_{48.42}Mn_{5.80}Fe_{2.08})O_{56.30}$. Accordingly, the total amount of Fe is equal to the sum of the Fe content of both solid solutions, i.e. 11.74. Though this result has been obtained by assuming the equilibrium re-distribution of Mn and Fe between both the solid solutions represented by eqns. (11) and (12), the value of 11.74 is very close to the $FeCO_3$ mole% of 11.27 in FeMn-dolomite as estimated by EPMA.

This agreement suggests that the equilibrium re-distribution of Mn and Fe is achieved at the second step of the decomposition.

As the Ca content of 48.42 is about 95% of the $CaCO_3$ mole% of 50.77 in the original FeMn-dolomite, the remaining ~ 5% of Ca has probably been recombined with $CO_2$ to produce $CaCO_3$ during cooling to room temperature without being incorporated in solid solutions. The existence of $CaCO_3$ at 906°C and 950°C, as shown in Fig. 5, supports this consideration.

After all, in this atmosphere, if Mn and Fe are supposed to behave like Mg, the first decomposition step of FeMn-dolomite will proceed similarly to

that of dolomite. Regarding the second decomposition step, FeMn-dolomite is more complicated than dolomite due to the formation of solid solutions as products, while the decomposition products of dolomite scarcely form solid solutions through its decomposition.

*$O_2$ partial pressures of the atmospheres in the experiments*

According to the foregoing results, Mn and Fe remain bivalent in CO 50%, while in CO 5%, though Mn remains bivalent, Fe is oxidized to the trivalent state. In $CO_2$, Mn is finally oxidized to tetravalent Mn and Fe to trivalent Fe. These differences in the valences of Mn and Fe result in the difference in the decomposition process of this mineral and then the products formed. Therefore, the oxidation states of Mn and Fe were examined thermodynamically in a similar manner to that in the case of magnesian kutnahorite [3,19].

Figures 9 and 10 show the equilibrium $O_2$ partial pressure curve at various temperatures in the systems Mn–O and Fe–O under 1 atm total pressure. The equilibrium $O_2$ partial pressures in $CO_2$, CO 5% and CO 50%, which were determined by dissociation of $CO_2$ into CO and $O_2$, are also shown in the figures. The estimation procedure was discussed in the previous paper on magnesian kutnahorite [3].

In Fig. 9, the $O_2$ partial pressure curve in CO 5% (C) is in the MnO stability region which is bounded by the equilibrium curves of Mn–MnO (1)

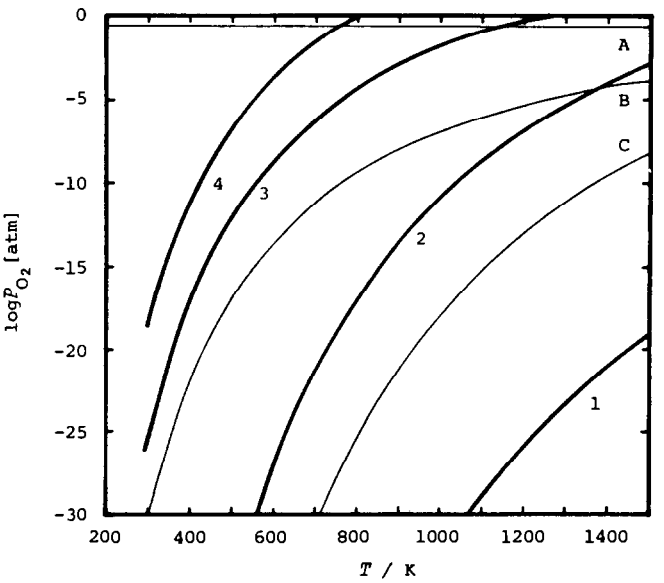


Fig. 9. Equilibrium $O_2$ partial pressure–temperature diagram in the system Mn–O under 1 atm total pressure. 1, 2 $MnO = 2\ Mn + O_2$; 2, 2 $Mn_3O_4 = 6\ MnO + O_2$; 3, 6 $Mn_2O_3 = 4\ Mn_3O_4 + O_2$; 4, 4 $MnO_2 = 2\ Mn_2O_3 + O_2$; A, $P_{O_2}$ in air; B, $P_{O_2}$ in $CO_2$; C, $P_{O_2}$ in CO 5%.

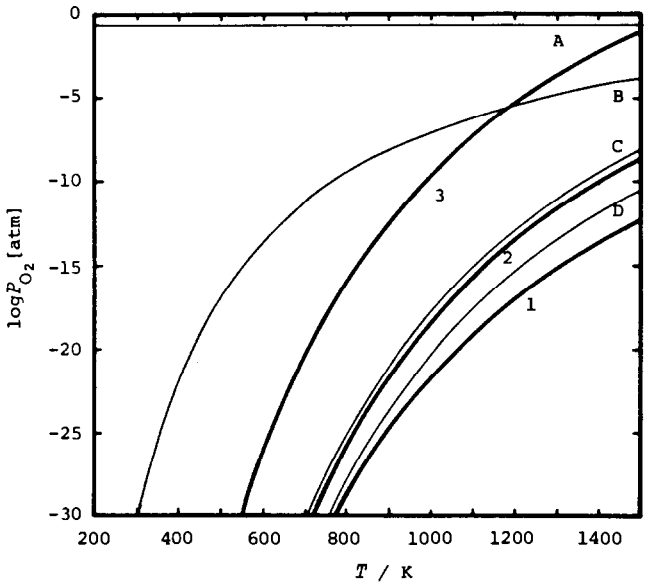


Fig. 10. Equilibrium $O_2$ partial pressure–temperature diagram in the system Fe–O under 1 atm total pressure. 1, 2 $FeO = 2\ Fe + O_2$; 2, 2 $Fe_3O_4 = 6\ FeO + O_2$; 3, 6 $Fe_2O_3 = 4\ Fe_3O_4 + O_2$; A, $P_{O_2}$ in air; B, $P_{O_2}$ in $CO_2$; C, $P_{O_2}$ in CO 5%; D, $P_{O_2}$ in CO 50%.

and $MnO–Mn_3O_4$ (2) showing that the formation of MnO is preferred in CO 5%. However, in Fig. 10, since the same curve (C) is above the $FeO–Fe_3O_4$ equilibrium curve (2), the oxidation of Fe to trivalent Fe will occur in the reaction process. Thus, in order to maintain Fe and Mn in the bivalent state, the CO 5% atmosphere is effective for Mn, but ineffective for Fe. On the other hand, the $O_2$ partial pressure curve in CO 50% (D) in Fig. 10 is in the FeO stability field bounded by the equilibrium curves of Fe–FeO (1) and $FeO–Fe_3O_4$ (2). Therefore, the $O_2$ partial pressure in CO 50% is low enough to maintain Fe as a bivalent cation.

These estimations can elucidate that FeMn-dolomite decomposes in two steps in a similar manner to dolomite in CO 50% because Mn and Fe behave like Mg as the stable bivalent cations, and that the two-step decomposition of FeMn-dolomite in CO 5% is not completely similar to that of dolomite because Fe is oxidized to the trivalent state and is excluded from the (Mg, Mn, Fe) group during decomposition. The essential condition, under which FeMn-dolomite decomposes in two steps like dolomite, is to maintain Mn and Fe in the bivalent state.

## CONCLUSIONS

Regarding the thermal decomposition of FeMn-dolomite, three different processes are observed in the three kinds of atmospheres.

In $CO_2$, in which the $O_2$ partial pressure is high enough to oxidize both Mn and Fe, FeMn-dolomite decomposes in three steps producing $CaCO_3$, $(Fe, Mn)_3O_4$ and MgO at the first step, $CaMnO_3$ and $CaFe_2O_4$ at the second and CaO at the third.

In CO 5%, the $O_2$ partial pressure is low enough to keep Mn in a bivalent state but sufficiently high to oxidize Fe to trivalent Fe. Under this condition, FeMn-dolomite decomposes in two steps producing $CaCO_3$, (Mg, Mn)O and $Fe_2O_3$ at the first step, and (Ca, Mn)O, (Mg, Mn)O and $Ca_2MgFe_2O_6$ at the second. However, the decomposition does not proceed like dolomite because of the oxidation of Fe in the (Mg, Mn, Fe) group.

In CO 50%, in which the $O_2$ partial pressure is sufficiently low to maintain both Mn and Fe as bivalent cations, FeMn-dolomite decomposes in two steps in a completely similar manner to dolomite itself. At the first step, $CaCO_3$ and (Mg, Mn, Fe)O, corresponding to $CaCO_3$ and MgO in the case of the decomposition of dolomite, are produced, and at the second step, (Ca, Mn, Fe)O is newly produced corresponding to CaO in the case of dolomite.

The only difference between FeMn-dolomite and dolomite is that, in the former, Mn and Fe are re-distributed at the second step decomposition between periclase and lime solid solutions until the equilibrium distribution is achieved.

## ACKNOWLEDGEMENTS

The authors thank Dr. Y. Ogasawara and Mr. N. Tomioka, Waseda University, for aid on EPMA analysis.

This study was partly supported by the Grant in Aid for the Scientific Research of the Ministry of Education, Japan (C-56550447).

## REFERENCES

1 R. Otsuka, S. Tanabe and K. Iwafuchi, J. Min. Metall. Inst. Jpn., 96 (1980) 581 (in Japanese).
2 R. Otsuka, S. Tanabe, K. Iwafuchi and R. Ozao, Proc. 6th Int. Conf. Therm. Anal., Bayreuth, Vol. 2, 1980, p. 295.
3 K. Iwafuchi, C. Watanabe and R. Otsuka, Thermochim. Acta, 60 (1983) 361.
4 H.A. Stalder, Schweiz. Mineral. Petrogr. Mitt., 44 (1964) 187.
5 W. Smykatz-Kloss, Beitr. Mineral. Petrogr., 9 (1964) 481.
6 D.N. Todor, Thermal Analysis of Minerals, Abacus Press, Tunbridge Wells, 1976, p. 180.
7 J.L. Kulp, P. Kent and P.F. Kerr, Am. Mineral., 36 (1951) 643.
8 C.W. Beck, Am. Mineral., 35 (1950) 985.
9 R. Otsuka and N. Imai, J. Min. Metall. Inst. Jpn., 84 (1968) 203 (in Japanese).
10 H.J. Van Hook and M.L. Keith, Am. Mineral., 43 (1958) 69.
11 A.H. Jay and K.W. Andrews, J. Iron Steel Inst., London, 152 (1945) 15.
12 R.C. Doman, J.B. Barr, R.N. McNally and A.M. Alper, J. Am. Ceram. Soc., 46 (1963) 313.

13 N. Tiberg and A. Muan, Metall. Trans., 1 (1970) 435.
14 R.H. Nafziger and A. Muan, Am. Mineral., 52 (1967) 1364.
15 W.C. Hahn, Jr. and A. Muan, Mater. Res. Bull., 5 (1970) 955.
16 K. Schwerdtfeger and A. Muan, Trans. Metall. Soc. AIME, 236 (1966) 201.
17 R.E. Johnson and A. Muan, Trans. Metall. Soc. AIME, 239 (1967) 1931.
18 J.B. Thompson, Jr., in P. Abelson (Ed.), Researches in Geochemistry, Vol. 2. Wiley, New York, 1967, p. 340.
19 R.A. Robie and D.R. Waldbaum, U.S. Geol. Surv. Bull., 1259 (1968).